Int. J. Electrochem. Sci., 16 **(2021)** 151005, doi: 10.20964/2021.01.14

International Journal of
ELECTROCHEMICAL
SCIENCE
www.electrochemsci.org

Short Communication

W and Mo Thin Films Electrodeposited from Aqueous Solutions

M. Saitou

University of the Ryukyus, Department of Mechanical Systems Engineering, 1 Senbaru Nishihara-cho Okinawa, 903-0213, Japan.
E-mail: saitou@tec.u-ryukyu.ac.jp

Received: 5 September 2020 / *Accepted:* 29 October 2020 / *Published:* 30 November 2020

Thin films electrodeposited from aqueous solutions containing W(VI) or Mo(VI) ions using rectangular pulse voltages with a 1 MHz frequency were investigated using scanning electron microscopy-energy dispersive X-ray (SEM-EDX) spectroscopy and X-ray diffraction (XRD). SEM-EDX analyses confirmed that the obtained thin films comprise W or Mo. The current efficiency increased with the cathode potential and tended to become constant, which is consistent with the phenomenological theory of electrodeposition. The potential barrier of W^{6+} and Mo^{6+} was 6.5 V and the maximum current efficiency (achieved by the W thin film) was 2.3 %. XRD analyses revealed that the W and Mo thin films have a body-centered cubic and amorphous structure, respectively.

Keywords: W and Mo thin films; Aqueous solution; Phenomenological theory; Body-centered cubic; Amorphous

1. INTRODUCTION

W and Mo thin films feature extensively in different research fields owing to their unique properties [1–2]. For example, W thin films demonstrate excellent wear resistance, corrosion resistance, and high hardness [3], whereas Mo thin films demonstrate the low contact resistance, low thermal expansion, and good chemical stability [4].

W and Mo electrodeposits have not been reported to form in aqueous solutions because of their relatively high negative standard electrode potentials and low hydrogen over-potentials [5–9]. However, the standard electrode potentials that account for thermal equilibrium cannot account for non-equilibrium phenomena associated with electrodeposition. Pure W and Mo thin films that form in non-aqueous solutions [10], such as organic solutions [11] and molten salts [12], have been previously investigated.

Additionally, W and Mo alloys can be easily electrodeposited when an aqueous solution contains iron group elements; this effect is called “induced co-deposition” [13] within the framework of thermal equilibrium. However, recent investigations have demonstrated that W and Mo alloys can also form in aqueous solutions free of iron group elements [14,15].

A phenomenological theory of electrodeposition that is not described by thermodynamic variables, but by the cathode potential, potential barrier, and resonant frequencies has been previously proposed [16]. Aqueous-solution based, electrodeposited thin films of Al (the metal has a large negative standard electrode potential, -1.662 V [17]) were not reported until recently, when, based on the phenomenological theory, Al thin films were electrodeposited in aqueous solutions [18]. This study demonstrates that W and Mo thin films can also be electrodeposited in aqueous solutions.

This study aims to demonstrate that thin films electrodeposited from aqueous solutions containing W(VI) or Mo(VI) comprised W and Mo, respectively. The current efficiency was consistent with the phenomenological theory, and the resultant W and Mo thin films had a body-centered cubic structure and amorphous structure, respectively.

2. EXPERIMENTAL SETUP

Aqueous solutions, A and B, were prepared with $Na_2WO_4 \cdot 2H_2O$ (0.5 mol L^{-1}) and $KNaC_4H_4O_6 \cdot 4H_2O$ (1mol L^{-1}), and $Na_2MoO_4 \cdot 2H_2O$ (0.5 mol L^{-1}) and $KNaC_4H_4O_6 \cdot 4H_2O$ (1 mol L^{-1}), respectively.

A 30 ×10 × 0.2 mm^3 copper plate and 50 × 40 × 1 mm^3 carbon plate were used as the cathode and anode, respectively. One side of the Cu plate was electrically insulated to prevent electrodeposition on this side. Two electrodes were placed parallel to each other in electrochemical cells filled with the prepared aqueous solutions. The temperatures of the solution were maintained at 300 K during electrodeposition.

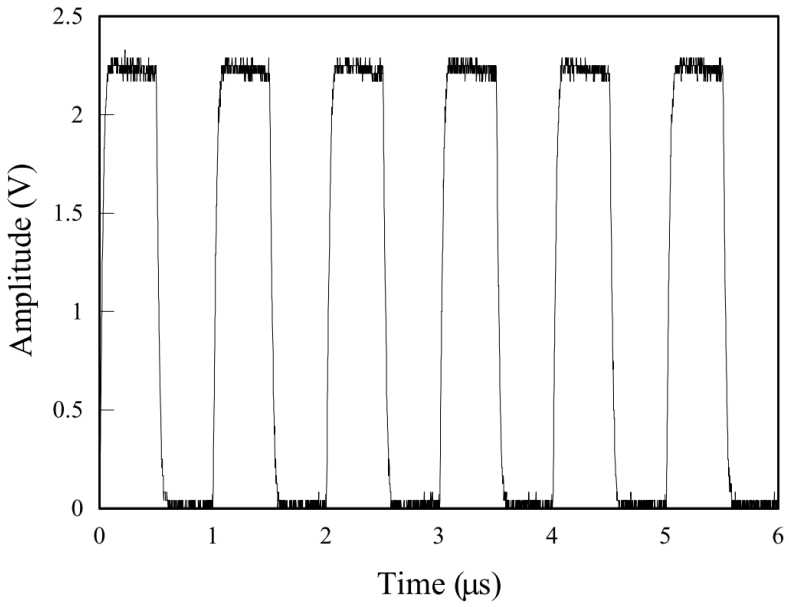

Figure 1. Voltage drops measured across a 22 Ω resistor when a rectangular pulse voltage with an amplitude of 9.2 V and frequency of 1.0 MHz was applied to the cell.

W and Mo thin films were electrodeposited on the Cu plates immersed to a depth of 10 mm in the respective solutions. The area of the C plate was approximately 40 times greater than that of the immersed Cu plate. Hence, the negligible impedance of the electric double layer in series with the C plate in the solution can be disregarded. The impedance between the cathode and anode can also be ignored owing to the use of highly concentrated aqueous solutions.

A rectangular pulse voltage with a frequency of 1MHz was supplied to the cell by a function generator. A 22 Ω metal film resistor was connected in series with the cell to determine the cathode potential (defined as the voltage applied to the electric double layer) and current flowing to the cell. The voltage drop across the metal film resistor was measured using a digital storage oscilloscope.

Figure 1 shows a typical rectangular pulse voltage measured across the metal film resistor when a rectangular pulse voltage with an amplitude of 9.2 V and frequency of 1.0 MHz is applied to the cell. The cathode potential was determined to be 7.0 V, which was the maximum cathode potential that could be supplied by the function generator used in this study.

The electrodeposits on the Cu plates were rinsed with distilled water and dried in a vacuum chamber after electrodeposition. The electrodeposits were weighed to a precision of 0.1 mg with an electric balance to calculate the current efficiency, defined as the ratio of the electrodeposited mass to the theoretical W or Mo mass expected to be liberated from the electrolyte by the current passing through the cell.

The electrodeposits on the Cu plates were investigated using scanning electron microscope-energy dispersive X-ray (SEM-EDX) spectroscopy (Hitachi TM3030). The crystallographic structure of the electrodeposits was determined by X-ray diffraction (XRD) using a diffractometer (Rigaku Ultima) with carbon-monochromator-filtered CuKα radiation.

3. RESULTS AND DISCUSSION

3.1 Determination of the thin film composition

Figure 2 shows the SEM images of the thin films and their compositions determined by SEM-EDX analysis. The thin film in Fig. 2 (a) was formed on a 10 × 10 mm^2 Cu surface at a cathode potential of 3.81 V from solution A. Based on EDX analysis, the thin film on the Cu surface comprises W. The W composition of the thin film within a circular area with a diameter of 1500 μm was 2.5 wt% based on the characteristic XRD results of the Cu plate and the electrodeposited thin film.

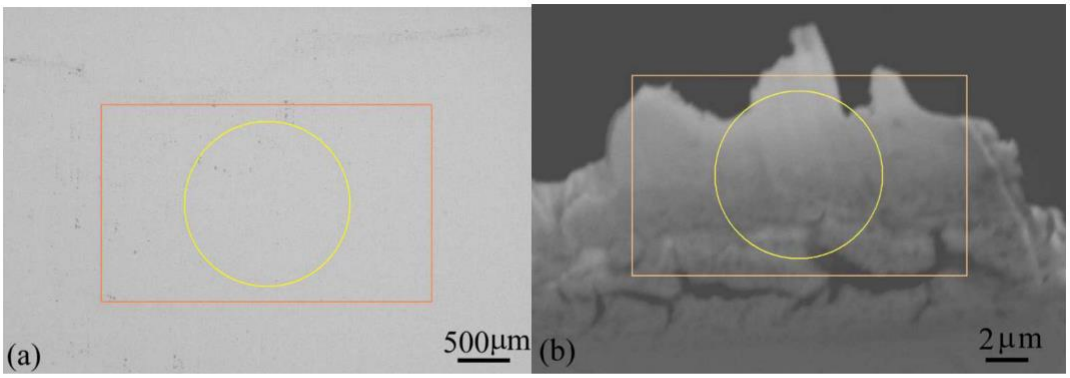

Element	[wt%]
Cu	97.5
W	2.5

Element	[wt%]
Cu	94.9
Mo	5.1

Figure 2. SEM images and contents of the thin films formed at a cathode potential of 3.81 V. (a) Thin film electrodeposited on a 10 ×10 mm^2 Cu surface from solution A. The W composition was determined within a circular area with a diameter of 1500 μm by SEM-EDX spectroscopy. (b) Detached thin film electrodeposited on a 10 × 0.2 mm^2 Cu end surface from solution B. The Mo composition was determined within a circular area with a diameter of 8 μm by SEM-EDX spectroscopy.

Figure 2 (b) shows a thin film separated from a 10 × 0.2 mm^2 Cu end surface, which was formed at a cathode potential of 3.81 V from solution B. The Mo composition of the thin film within a circular area with a diameter of 8 μm is 5.1 wt%. Figure 2 confirms the presence of W and Mo in the thin films. The W and Mo contents of the electrodeposits formed at cathode potentials of 2, 3.81, 5.8, 6.5, and 7 V were measured in two different regions of the same thin films. W and Mo were detected in all the associated electrodeposits. Oxygen was not detected in the W and Mo thin films. As shown in Fig. 1, current passes for 0.5 μs during each cycle. Electrochemical reactions that require > 0.5 μs do not contribute to the reduction processes of $[WO_4]^{-2}$ and $[MoO_4]^{-2}$. Instead of investigating equilibrium processes of the reduction of $[WO_4]^{-2}$ and $[MoO_4]^{-2}$ [8–9, 19], further studies should focus on time-dependent reduction processes.

3.2 Crystallographic structures of W and Mo thin films

Figure 3 shows a typical XRD pattern of a 0.4 μm-thick W thin film electrodeposited at a cathode potential of 7.0 V from solution A. A weak diffraction peak from the (200) planes of the W thin film [20] is observed. No other W-associated diffraction peaks were observed. The (200) diffraction peak indicates that the W thin film has a body-centered cubic (BCC) structure and that the (200) crystallographic growth plane was parallel to the Cu plane.

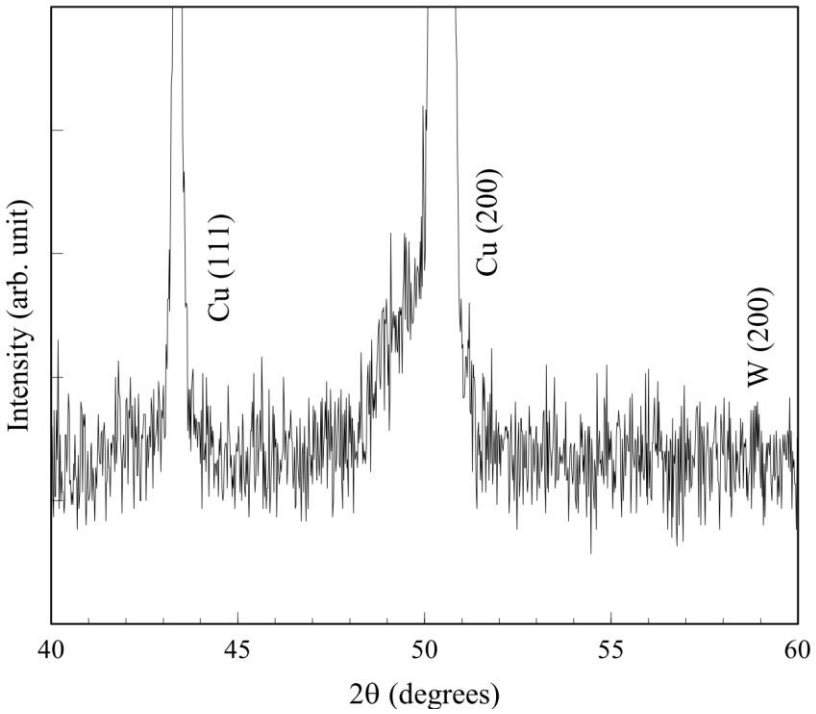

Figure 3. XRD pattern of a 0.4 μm-thick W thin film electrodeposited at a cathode potential of 7.0 V from solution A.

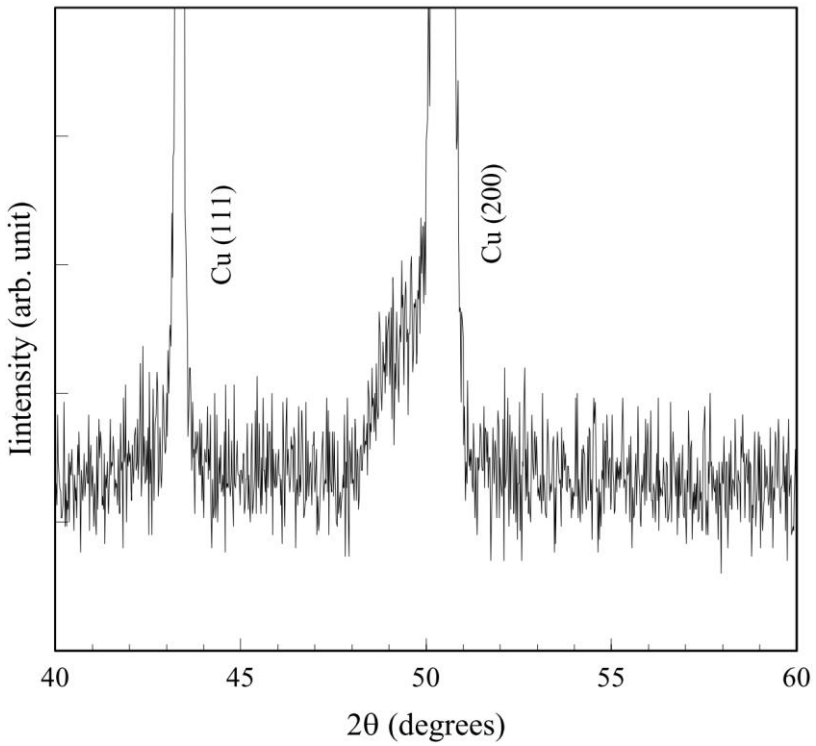

Figure 4. XRD pattern of a 0.5 μm-thick Mo thin film electrodeposited at a cathode potential of 7.0 V from solution B.

Figures 4 shows a typical XRD pattern of a 0.5 μm-thick Mo thin film electrodeposited at a cathode potential of 7.0 V from solution B. No diffraction peaks associated with the Mo thin films are observed, indicating that the Mo thin film has an amorphous structure [21].

3.3 Surface morphology of W and Mo thin films

Figure 5 shows SEM images of the W and Mo thin films electrodeposited on Cu plates at cathode potentials of 2.0 and 7.0 V, respectively. The surface morphology of the W thin film in Fig. 5 (a) is characterized by steps, terraces, and kinks. It is inferred that the steps are bundled during electrodeposition and achieve a step height suitable for observation by SEM.

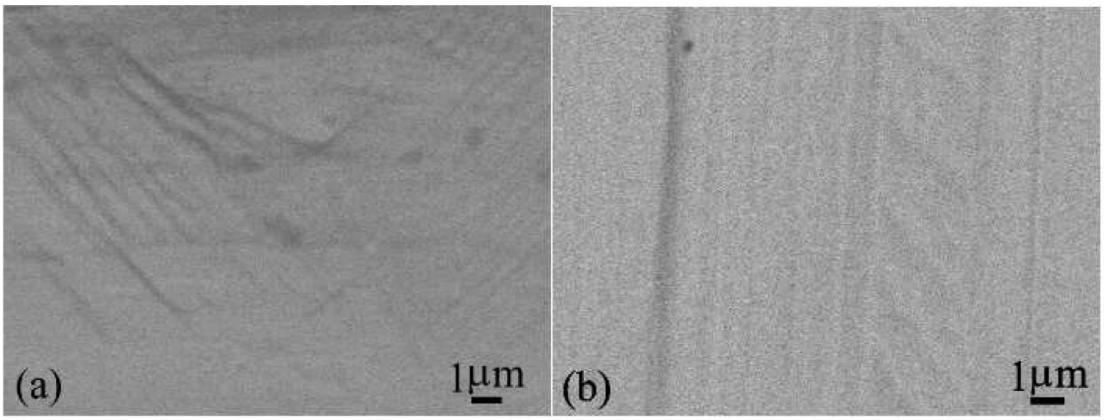

Figure 5. SEM images of (a) a W thin film electrodeposited at a cathode potential of 2.0 V from solution A, and (b) a Mo thin film electrodeposited at a cathode potential of 7.0 V from solution B.

The surface does not comprise islands [5] but appears to have formed by the layer-by-layer via the Burton-Cabrera-Frank surface growth mechanism [22]. The surface morphology of the Mo thin film in Fig. 5 (b) is characterized by steps, terraces, and kinks similar to the film in Fig. 5 (a). The Mo surface appears to be smooth. There are no cracks in the W and Mo thin films formed on the Cu surfaces [11].

3.4 Dependence of the current efficiency on the cathode potential

Figure 6 shows the dependence of the current efficiency on the cathode potential. According to the phenomenological theory of electrodeposition [16, 18], the current efficiency increases with the cathode potential and intends to becomes constant when the cathode potential exceeds the potential barrier of W^{+6} and Mo^{6+}. The dependence of the current efficiency on the cathode potential in Fig. 6 is consistent with that in the phenomenological theory.

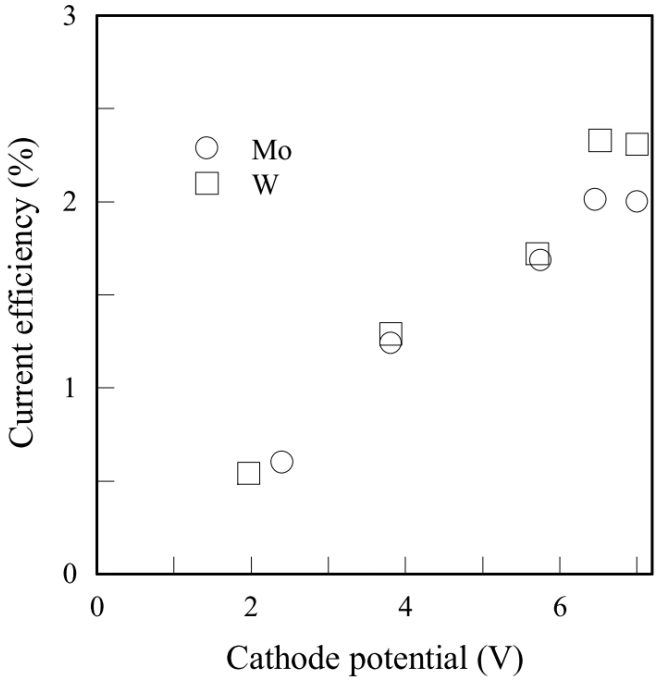

Figure 6. Dependence of the current efficiency of the electrodeposited W and Mo thin films on the cathode potential.

The potential barriers of W^{+6} and Mo^{6+} were determined to be 6.5 V, which value is much higher than those of Fe^{2+}, Mn^{2+}, Co^{2+}, Ni^{2+}, and Al^{3+} [16, 18]. Hence, W^{+6} and Mo^{6+} ions have a lower probability of atomization than Fe^{2+}, Mn^{2+}, Co^{2+}, Ni^{2+}, and Al^{3+}ions. The constant current efficiency of the Mo thin films was slightly lower than the constant current efficiency of 2.3 % of the W thin films.

4. CONCLUSIONS

The compositions of thin films electrodeposited from solutions A and B were identified as W and Mo, respectively, using SEM-EDX analysis. The current efficiency of the W and Mo thin films increased with the cathode potential and tended to become constant. The potential barriers of W^{6+} and Mo^{6+} were determined to be 6.5 V and the maximum current efficiency of the W thin films was 2.3 %. These results are consistent with the phenomenological theory of electrodeposition. The XRD analyses revealed that the W and Mo thin films have a BCC and amorphous structure, respectively.

References

1. M. B. Porto, VdL. Bellia, T. CdM. Nepel, F. L. Moreira, and A. FdA. Neto, *J. Mater. Res. Technol.*, 8 (2019) 4547.
2. M. M. Aqil, M. A. Azam, M. F. Aziz, and R. Latif, *J. Nanotecnol.*, (2017) 4862087.
3. F. Zhu, Z. Xie, and Z. Zhang, *AIP Adv.*, 8 (2018) 035321.
4. M. Khan and M. Islam, *Semiconductors.*, 47 (2013) 1610.
5. E. Yoo, A. Y. Samardak, Y. S. Jeon, A. S. Samardak, A. V. Ognev, S. V. Komogortsev, and Y. K.

Kim, *J. Alloys Compd.*, 843 (2020) 155902.
6. N. Tsyntsaru, *Russ. J. Electrochem.*, 52 (2016) 1041.
7. T. Maliar, H. Cesiulis, and E. J. Podlaha, *Front. Chem.*, 7 (2019) 542.
8. L. Ma, X. Xi, Z. Nie, T. Dong, and Y. Mao, *Int. J. Electrochem. Sci.*, 12 (2017) 1034.
9. A. Hara, Z. Świątek, and P. Ozga, *J. Alloys Compd.*, 827 (2020) 154195.
10. W. Simka, D. Puszczyk, and G. Nawrat, *Electrochim. Acta*, 54 (2009) 5307.
11. M. G. Zacarin, M. M. de Brito, E. P. Barbano, R. M. Carlos, V. R. Mastelaro, and I. A. Carlos, *J. Alloys Compd.*, 750 (2018) 577.
12. Q. Zhang, X. Xi, W. Qin, L. Zhang, L. Ma, and Z. Nie, *Int. J. Electrochem. Sci.*, 14 (2019) 11092.
13. A. Brenner, *Electrodeposition of Alloys,* New York, Academic Press, (1963).
14. M. Saitou, *Int. J. Electrochem. Sci*., 12 (2017)1193.
15. M. Saitou, *Int. J. Electrochem. Sci.*, 12 (2017) 4714.
16. M. Saitou, *Int. J. Electrochem. Sci.*, 15 (2020) 6561.
17. D. R. Lide, *CRC Handbook of Chemistry and Physics*, 79th ed., New York, CRC Pr., (1998).
18. M. Saitou, *Int. J. Electrochem. Sci.*, 15 (2020) 10971.
19. E. Eliaz and E. Gileadi, *Etc Trans*., 2 (2007) 337.
20. W. Qin, X. Xi, Q. Zhang, L. Zhang, L. Ma, and Z. Nie, *Int. J. Electrochem. Sci.*, 14 (2019) 10420.
21. R. Syed, S. K. Ghosh, P. U. Sastry, G. Sharma, R. C. Hubli, and J. K. Chakravartty, *Surf. Coat. Technol.*, 261 (2015) 15.
22. W. K. Burton, N. Cabrera, and F. C. Frank, *Phil. Trans. R. Soc. Lond. Ser. A*, 243 (1951) 299.